A Numerical Method for the Topological Analysis of the Laplacian of the Electronic Charge Density in Molecules and Solids

Yosslen Aray,* Jesús Rodríguez, and Roberto López-Boada

Centro de Química, IVIC, Apartado 21827, Caracas 1020A, Venezuela

Received: August 7, 1996; In Final Form: October 25, 1996[⊗]

A numerical method that analyzes the topology of the Laplacian of the electronic density regardless of how it was obtained (analytically, numerically, or even experimentally) was implemented for the BUBBLE program. The method allows the study of a complex system where the electronic correlation is important, by density functional theory regardless the kind of basis set used, and allows the analysis of the Laplacian of the resulting charge density with the topological theory of Bader. The method was applied to CO and NO molecules and the Cu_{13}, Cu_{45}, and Fe_{21} clusters modeling the (100) Cu and (001) Fe surfaces, respectively.

Introduction

Density functional theory (DFT) plays a role of increasing importance in the calculations of ground states of molecules and solids.[1−9] The inclusion of the electron correlation effects is necessary for an accurate description of many electron systems.[2] By standard methods, such as configuration interaction, perturbation or the Green function theory, the inclusion of the electron correlation for an extended system is a very difficult matter.[2] However, this problem is overcome with the appearance of DFT, in which the correlation is included by introducing a local (or nonlocal) approximation for a functional of the electronic density that describes the correlation effects. The practical implementations of DFT lead to the Kohn and Sham (KS) equations.[2] Their solution has no more numerical difficulties than the Hartree equations. This allows us to handle complex systems such as solids, surfaces, interfaces, transition metals, and organometallic compounds.[6,8] Additionally, the DFT methods are not restricted to traditional Gaussian basis set functions[6] since it is possible to use different sets such as muffin tin orbitals, multiple scattering, plane waves, or numerical functions.

The topological theory of Bader is very useful to extract the chemical information from the charge density.[10−30] The reactivity of molecules is reflected in the topology of the Laplacian of the charge density $\nabla^2\rho$.[20−23] The Laplacian of any scalar field, such as $\rho(\mathbf{r})$, determines where the field is locally concentrated ($\nabla^2\rho < 0$) and locally depleted ($\nabla^2\rho > 0$).[10] Since electron density is concentrated where $\nabla^2\rho < 0$, the topology of the Laplacian is conveniently given in terms of $-\nabla^2\rho$. The atomic Laplacian[24,25] exhibits alternating shells of charge concentration and charge depletion equal in number to the number of quantum shells. The outer valence shell of charge concentrations (VSCC) contains a spherical surface over which $\rho(\mathbf{r})$ is maximally concentrated. The distribution of the $-\nabla^2\rho$ over this surface in the free atom is uniform if one assumes that the nucleus has a negligible electric quadrupole moment. In general, this surface persists when the atom is in chemical combination but the surface is no longer spherical and has no longer a uniform concentration. The formation of bonds produces changes in this distribution, and a number of local maxima, minima, and saddles appear in this surface of charge distribution.[22] The localized concentrations of charge mimic in number, relative position, and size the pairs of electrons assumed in the Lewis model, topological features that are absent from the relatively simple topology exhibited by the density itself. The structure of the VSCC for an atom in a molecule,[22,23] called its atomic graph, is most easily visualized in terms of the polyhedron defined by the maxima in $-\nabla^2\rho$, a polyhedron whose vertices (V), edges (E), and faces (F) satisfy Euler's formula:

$$V - E + F = 2$$

The maxima define the vertices, V, the unique pairs of $\nabla(\nabla^2\rho)$ trajectories that originate at $(3, -1)$ critical points and terminate at neighboring vertices define the edges, E, and the $(3, +1)$ critical points define the faces, F. The face critical points define the centers of local depletions in the valence shell charge concentration. A Lewis acid−base reaction corresponds to aligning a charge concentration (CC) of the VSCC on the base with a charge depletion (CD) on the acid, that is, by directing a vertex of the graph on the base atom at a face of the polyhedron on the acid. This is a general phenomenon that is observed in many different kinds of interactions,[10] examples being the formation of hydrogen bonds,[26] the alignment of chlorine molecules in the solid,[16] and the adsorption of molecules on surface.[27−30] The Laplacian of the electronic density provides a physical model that guides us in the determination of the sites of adsorption, the geometry of approach of the reactant relative to the surface site, and predicts whether the interaction will correspond to physi- or chemisorption.[27] A recent study,[30] using molecular orbital Hartree−Fock, post-Hartree−Fock at MP2 and QCISD levels and DFT calculations has confirmed that the DFT methods provide a good description of the topology of Laplacian of the electronic density. Unfortunately, the available algorithms for the toplogical analysis of $\nabla^2\rho$ (BUBBLE,[31] GAUSSIAN[32,33] 94, MORPHY,[34] and TOPOND[35] program in CRYSTAL[36] 95) have been only implemented for analytical Gaussian basis sets. This limits the applicability of the Laplacian topology in many interesting systems in which the correlation effects play an important role. Due to the existence of a large variety of software employing different basis set and the unavailability of the source code in commercial cases, in the present work, a numerical method was developed that is able to analyze the topology of the Laplacian of the electronic density regardless of how $\rho(\mathbf{r})$ was generated (analytically, numerically, or even experimentally). The method allows one to study complex systems by DFT and analyze the resulting density with the topological theory of Bader. In the present study, this method was implemented as a modification to the BUBBLE[31] program and applied to CO and NO molecules plus some Cu and Fe clusters. It would be equally simple to adapt the method to other available programs.

[⊗] Abstract published in *Advance ACS Abstracts,* February 1, 1997.

S1089-5639(96)02390-0 CCC: $14.00

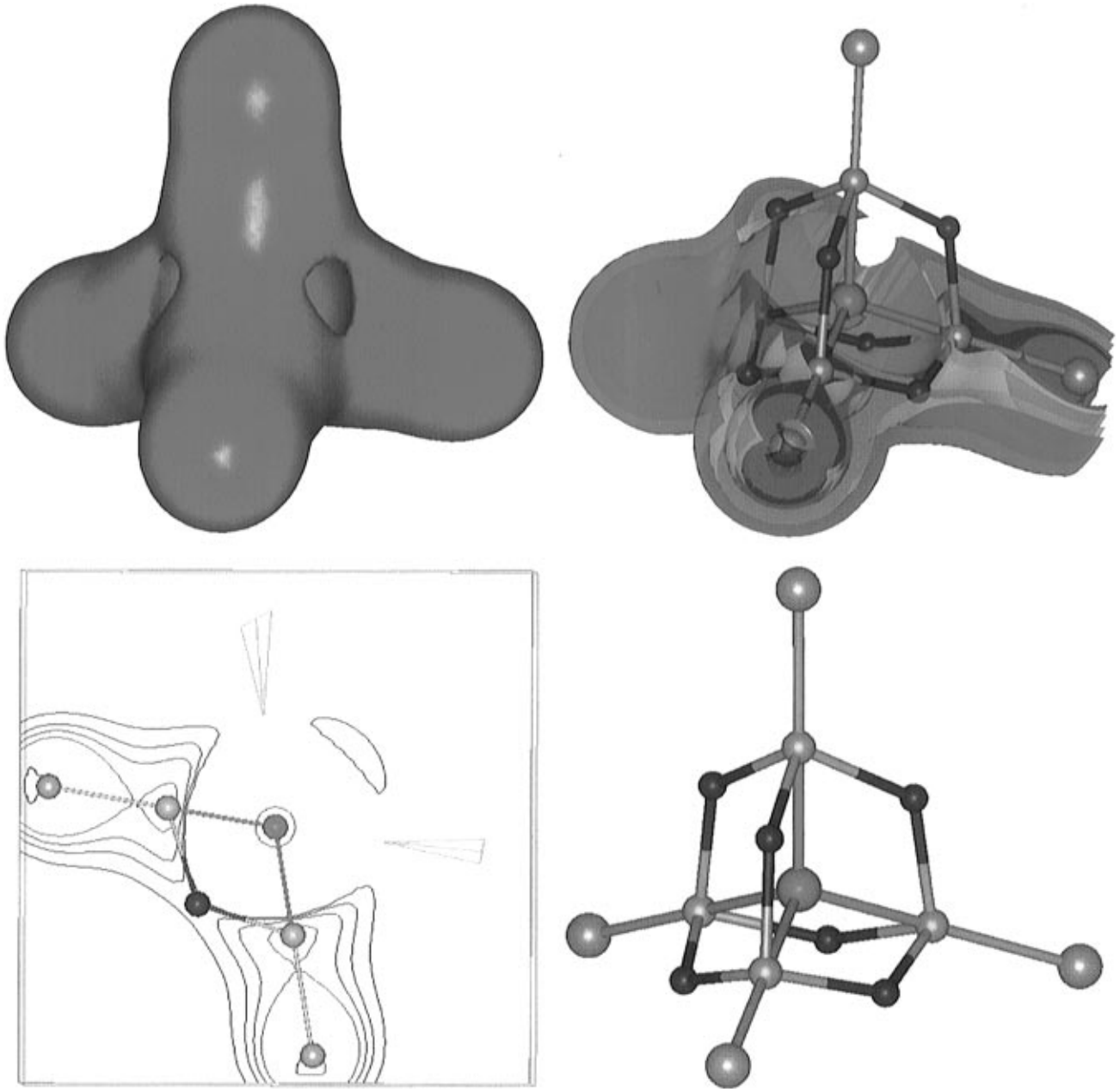

Figure 1. (a, top left) Zero envelope of the Laplacian of the charge density for methane. This envelope separates the regions of charge concentrations from those of charge depletion. Note the presence of the pronounced holes at the position of the carbon atom. These holes correspond to the (3, +1) critical points. (b, top right) Three-dimensional cross section showing the structure of the methane VSCC. Green and white spheres denote the position of the carbon and hydrogen nucleus, respectively. Red, pink, orange, sky blue and purple surfaces correspond to contour values of 0.1, 0.5, 0.8, 1.5, and 2.0 au, respectively. Yellow and blue spheres mark the (3, −3) critical points or local charge concentration and (3, −1) saddles points, respectively. (c, bottom left) Contour plot of $-\nabla^2\rho$ in a plane containing the carbon and two hydrogen nuclei. The contour (red lines) values in au are 0.1, 0.5, 0.8, 1.5, and 2.0. The outermost contour in each plot is 0.1. The (3, −3) critical points are denoted by yellow spheres while the (3, −1) ones are denoted by blue spheres. The arrows point out the (3, +1) critical points at the graph faces. (d, bottom right) Atomic graph for the carbon atom, a tetrahedron with four curved faces. There is a (3, −3) critical point in $-\nabla^2\rho$, at each vertex denoted by a yellow sphere, and a (3, −1) critical point defining each edge indicate by a blue sphere.

Theory

The properties of a scalar field such as $-\nabla^2\rho$ are summarized in terms of its critical points (CP).[10] These are points where the gradient vector field, $\nabla(-\nabla^2\rho)$, vanishes and are classified by the $-\nabla^2\rho(\mathbf{r})$ curvatures or three eigenvalues λ_i (i = 1, 2, and 3) of the Hessian matrix ($H_{ij} = \partial^2\nabla^2\rho/\partial x_i\partial x_j$). There are,[22] in the surface of the VSCC, three types of these extremes that labeled by their rank (number of nonzero eigenvalues) and signature (excess number of positive over negative eigenvalue) are (3, −3), (3, +1), and (3, −1). The curvature[22] of $-\nabla^2\rho$ normal to this surface, the radial curvature, is negative while the two tangential curvatures can assume either positive or negative values. If both of those curvatures are negative or positive then a local maximum, a (3, −3) CP, or local minimum, a (3, +1) CP, is formed on that surface, respectively. When one of the tangential curvatures is negative and the other positive a saddle, a (3, −1) CP will be formed. Each maximum[22] is linked to the another one by unique pairs of trajectories of the gradient of $-\nabla^2\rho$ which originate at the saddle points. The network of those trajectories partitions the surface of charge concentration in segments with curved faces. In the center of each face there is a local minimum in the surface of the VSCC. This structure is called an atomic graph[22] and succinctly summarizes the type and number of the CPs formed on the surface of charge concentration of an atom in a molecule. This graph provides the connectivity of the extremes of the $-\nabla^2\rho$ in

the corresponding surface of charge concentration of the VSCC distribution. In the C atom of the methane molecule (Figure 1), for example, the VSCC exhibits four local charge concentrations or (3, −3) CPs, each one lying along the C−H bonds, linked by six (3, −1) CPs defining four faces with one (3, +1) CP in the center of each face. Thus, the atomic graph for that atom is a regular tetrahedron with four triangular curved faces (Figure 1d). The values of the $-\nabla^2\rho$ at the (3, −3), (3, −1), and (3, +1) are 1.190, 0.234, and −0.119 au, and the distances from the nucleus are 0.982, 0.968, and 1.003 au, respectively. As we can see, the charge distribution on the VSCC shows large changes while the distances from the nucleus only show slight differences. In general, the surface of charge concentration is almost spherical and the value of its radius is characteristic of the nature of the atom. The number, type, location, and $-\nabla^2\rho$ value of the critical points on that surface are a function of the linked atoms.

Methodology

BUBBLE determines the critical points of $-\nabla^2\rho$ based on the Newton−Raphson (NR) technique.[37] The NR algorithm starts from a truncated Taylor expansion at a point $\mathbf{r} = \mathbf{r}_0 + \mathbf{h}$, about $\mathbf{r}_0$ of a multidimensional scalar function,

$$-\nabla^2\rho = -\nabla^2\rho_0 + \mathbf{g}^T\mathbf{h} + (^1/_2)\mathbf{h}^T\mathbf{H}\mathbf{h} \qquad (1)$$

where $-\nabla^2\rho$ is the Laplacian of the electron density and **g** and **H** are its gradient and Hessian (matrix) at point $\mathbf{r}_0$, respectively. The best NR step **h** to get from the initial $\mathbf{r}_0$ to the critical point is $\mathbf{h} = -\mathbf{H}^{-1}\mathbf{g}$. This correction is then used to obtain the new starting point $\mathbf{r}_{new}$, and the process is iterated to $\nabla(-\nabla^2\rho) = 0$. The NR algorithm requires the evaluation of the first, second, third, and fourth partial derivatives of ρ at arbitrary points **r**. The BUBBLE program evaluates these derivatives analytically, using a Gaussian basis representation for the electronic density.

In the present work, we represented ρ on to a homogeneous grid of interval size h and use standard numerical methods[37] to calculate the partial derivatives of ρ, which are then used in the NR algorithm. Our methodology consists of performing all calculations on an uniform grid of the electronic density. In a simple approach, we have used finite difference approximations to the partial derivatives for equally spaced base points. In this method the derivative expressions are developed as a linear combination of its functional values. For example, the forward first derivative approximation of a $f(x)$ function at the x_i point usiong a fourth-order polynomial is evaluated by expanding the Taylor series about points x_i, x_{i+1}, x_{i+2}, x_{i+3}, and x_{i+4}. Thus,

$$f'(x_i) = (^1/_2h)[-3f(x_i) + 4f(x_i + 1) - f(x_i + 2)] + (h^2/3)f'''(x_i) + (h^3/4)f^{iv}(x_i) \qquad (2)$$

where h is the separation step between the points. If f' is truncated at the third derivative, the error can be assumed to be of order h^2 and is represented by $(O)h^2$. Therefore f' is given as

$$f'(x_i) = (^1/_2h)[-3f(x_i) + 4f(x_i + 1) - f(x_i + 2)] + O(h^2) \qquad (3)$$

This expression can be simplified in the so called "stencil" form[37] considering only the significant features such as the direction, functional values, coefficients, and order of error. Thus, the eq 2 in the stencil representation is expressed as,

$$f' = (^1/_2h)\left(\textcircled{\textcircled{-3}}\ \ 4\ \ -1\right) + O(h^2) \qquad (4)$$

Such expressions include only the coefficients of the functional values present in the derivative formulas. The double circles indicate the position of the base point where the derivative is being evaluated, and the adjacent circles are separated by the interval h.

In this work, we have developed derivative expressions with eighth-order error ($O(h^8)$) and backward, forward, and central interpolation. For example, using the stencil form, the approximation formulas developed for the case of central interpolation, to determine the noncrossed first, second, third, and fourth derivatives of ρ and the mixed partial derivative, such as $\partial^4\rho/\partial^2x\partial^2y$ (due to the expression involving an error of $O(h^8)$, it is just too large (an 11 × 11 matrix), we have chosen one with an error of $O(h^4)$ as illustrative), are

$$\frac{\partial\rho}{\partial\omega} = \left(\frac{1}{840h}\right)\left(\textcircled{3}\ -32\ 168\ -672\ \textcircled{\textcircled{0}}\ 672\ -168\ 32\ -3\right) \qquad (5)$$

$$\frac{\partial^2\rho}{\partial\omega^2} = \left(\frac{1}{10\,080h^2}\right)\left(\textcircled{-9}\ 128\ -1008\ 8064\ \boxed{-14\,350}\ 8064\ -1008\ 128\ \textcircled{-9}\right) \qquad (6)$$

$$\frac{\partial^3\rho}{\partial\omega^3} = \left(\frac{1}{181\,440h^3}\right)\left(-205\ 2522\ -14\,607\ 52\,428\ -70\,098\ \textcircled{\textcircled{0}}\ 70\,098\ -52\,428\ 14\,607\ -2522\ 205\right) \qquad (7)$$

$$\frac{\partial^4\rho}{\partial\omega^4} = \left(\frac{1}{362\,880h^4}\right)\left(\textcircled{82}\ -1261\ 9738\ -52\,428\ 140\,196\ \boxed{-192\,654}\ 140\,196\ -52\,428\ 9738\ -1261\ \textcircled{82}\right) \qquad (8)$$

$$\frac{\partial^4\rho}{\partial\omega^2\partial\beta^2} = \frac{\partial^2}{\partial\omega^2}\left(\frac{\partial^2}{\partial\beta^2}\right) = \frac{1}{12h^2}\begin{Bmatrix}-1\\16\\-30\\16\\-1\end{Bmatrix}\{-1\ 16\ -30\ 16\ -1\}\frac{1}{12h^2} = \frac{1}{12^2h^4}\begin{Bmatrix}1&-16&30&-16&1\\-16&256&-480&256&-16\\30&-480&\textcircled{\textcircled{900}}&-480&30\\-16&256&-480&256&-16\\1&-16&30&-16&1\end{Bmatrix} \qquad (9)$$

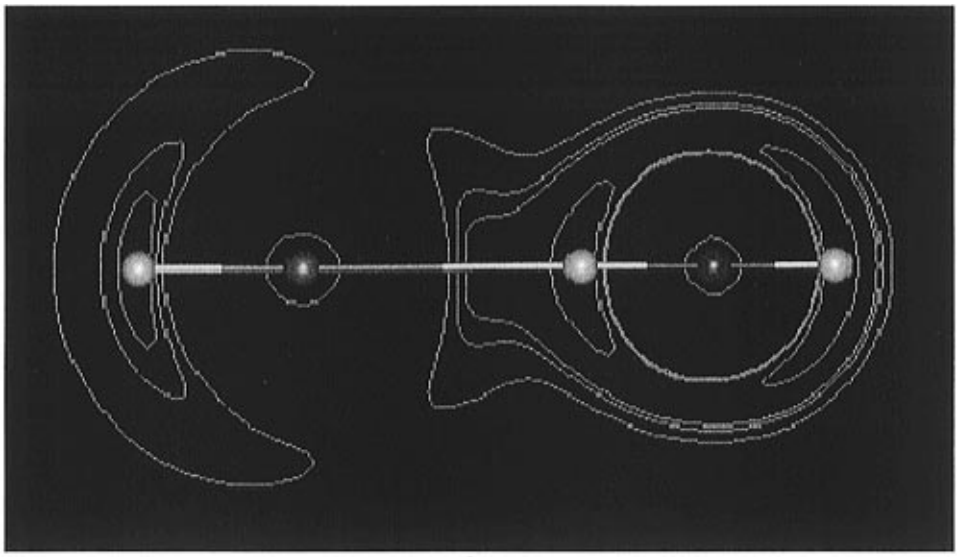

2a

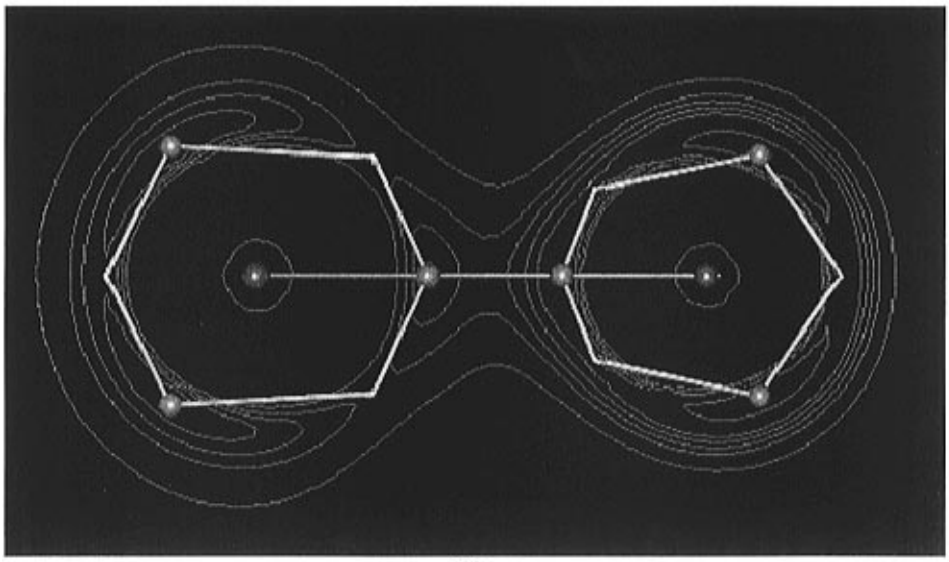

2b

Figure 2. Laplacian distribution for (a) carbon monoxide and (b) nitrogen monoxide. Only contours for $-\nabla^2\rho$, that is, concentration of electronic charge are plotted. The contour values in au are 0.1, 1.0, 2.0, 3.0, and 4.0. The outermost contour in each plot is 0.1. The (3, −3) critical points or local charge concentrations are denoted by white spheres in the middle of the lobes. In panel b there is also (3, −1) CPs located at the leftmost hexagon at 2, 4, and 9 o'clock, and in the rightmost hexagon at 3, 8, and 11 o'clock.

where ω and β are the coordinates x, y, or z.

The additional computational load of the proposed method was found to be not greater than that of preparing a grid-based plot. However, this load can be significantly longer than that required by the analytical approaches. Once that grid is built, one needs to calculate the derivatives of ρ at the *same* number of arbitrary points $\mathbf{r}_i$ in both methods. In order to to carry out the topological analysis within an atomic VSCC, the BUBBLE program samples angular, azimuthal, and radially in a spherical shell of radius varying from R_i to R_f around the shell characteristic atomic radius R. In general, around 1400 points ($n_i = 14$ (angular points) $\times$ 10 (θ points) $\times$ 10 (radius points)) are enough for an exhaustive topological analysis with this program. The analytical method calculates the values of the derivatives only at the $\mathbf{r}_i$ points using the basis functions while the numerical one instead has to use equations such as 5−9. Such equations involve *several* points around each $\mathbf{r}_i$, and the program has to interpolate when the points are not on the grid. The additional number of points required by the numerical approach is given by $[(4/3)\pi(R_f^3 - R_i^3)/h^3] - n_i$. For example, in a N atom, where R_i and R_f can be 0.74 and 0.86, respectively, the additional number of points needed are 34 411 when $h = 0.03$ or 119 463 when $h = 0.02$.

TABLE 1: Data for $-\nabla^2\rho(\mathbf{r})$ at the (3, −3) Critical Points in the Atomic Valence Shell of the CO Molecule

O atom				
	bonded		nonbonded	
step	$-\nabla^2\rho$	$\mathbf{r}_O$	$-\nabla^2\rho$	$\mathbf{r}_O$
analytic	4.477 105 49	0.691 728 87	4.746 419 80	0.641 029 94
0.04	4.477 131 87	0.691 710 16	4.746 493 54	0.641 013 70
0.03	4.477 108 72	0.691 727 06	4.746 424 76	0.641 028 02
0.02	4.477 105 72	0.691 728 98	4.746 420 27	0.641 029 89

C atom		
	nonbonded	
step	$-\nabla^2\rho$	$\mathbf{r}_C$
analytic	1.259 823 60	0.857 275 40
0.04	1.259 824 59	0.857 274 78
0.03	1.259 823 72	0.857 275 40
0.02	1.259 823 11	0.857 275 50

TABLE 2: Data for $-\nabla^2\rho(\mathbf{r})$ at the Critical Points in the Atomic Valence Shell of the NO Molecule

N atom				
(3, −3)				
	nonbonded, V_1 and V_2		V_{bonded}	
step	$-\nabla^2\rho$	$\mathbf{r}_N$	$-\nabla^2\rho$	$\mathbf{r}_N$
analytic	2.518 458 89	0.742 211 85	1.869 794 60	0.835 319 97
0.04	2.518 459 56	0.742 209 05	1.869 802 12	0.835 326 05
0.03	2.518 458 95	0.742 211 45	1.869 794 75	0.835 324 06
0.02	2.518 458 91	0.742 211 83	1.869 794 50	0.835 320 89
(3, −1)				
	bonded, E_1 and E_2		$E_{nonbonded}$	
step	$-\nabla^2\rho$	$\mathbf{r}_N$	$-\nabla^2\rho$	$\mathbf{r}_N$
analytic	0.976 695 85	0.794 687 25	2.100 135 26	0.743 188 21
0.04	0.976 696 11	0.794 689 43	2.100 144 63	0.743 257 94
0.03	0.976 695 87	0.794 687 65	2.100 136 53	0.743 200 09
0.02	0.976 695 84	0.794 687 29	2.100 134 76	0.743 189 21
(3, +1)				
	F_1, F_2			
step	$-\nabla^2\rho$	$\mathbf{r}_N$		
analytic	0.100 042 38	0.862 741 66		
0.04	0.100 041 80	0.862 739 37		
0.03	0.100 042 42	0.862 740 97		
0.02	0.100 042 08	0.862 741 27		
O atom				
(3, −3)				
	nonbonded, V_1 and V_2		V_{bonded}	
step	$-\nabla^2\rho$	$\mathbf{r}_O$	$-\nabla^2\rho$	$\mathbf{r}_O$
analytic	5.097 113 79	0.642 765 14	3.236 256 29	0.714 323 03
0.04	5.097 117 93	0.642 776 66	3.236 274 98	0.714 379 53
0.03	5.097 113 97	0.642 765 25	3.236 258 00	0.714 321 58
0.02	5.097 113 46	0.642 765 14	3.236 257 35	0.714 323 01
(3, −1)				
	bonded, E_1 and E_2		$E_{nonbonded}$	
step	$-\nabla^2\rho$	$\mathbf{r}_O$	$-\nabla^2\rho$	$\mathbf{r}_O$
analytic	2.751 220 88	0.689 396 47	3.839 196 48	0.650 475 59
0.04	2.751 222 26	0.689 401 26	3.839 229 63	0.650 614 11
0.03	2.751 220 98	0.689 397 37	3.839 201 24	0.650 497 38
0.02	2.751 220 87	0.689 396 47	3.839 196 99	0.650 475 47
(3, +1)				
	F_1, F_2			
step	$-\nabla^2\rho$	$\mathbf{r}_O$		
analytic	1.595 911 22	0.702 367 89		
0.04	1.595 920 35	0.702 376 48		
0.03	1.595 911 12	0.702 369 24		
0.02	1.595 911 08	0.702 367 88		

Results and Discussion

The accuracy of the numerical evaluation of the topological properties of the $-\nabla^2\rho$ at the critical points with the modified version of BUBBLE (called NUMLAP) was tested by comparing the results of Gaussian 94 analytic KSOs using the original BUBBLE program and the results using a numerical grid of ρ, calculated with the CUBEV program of the AIMPAC 94 package.[31] CUBEV builds a homogeneous grid of ρ of step size h. The analytical KS orbitals were calculated using the gradient-corrected Becke exchange potential[38] together with the correlation potential of Lee, Yang, and Parr[39] (BLYP) and the 6-311G** Gaussian basis set.[40] An error of order of h^8 is expected for the partial derivatives associated with the difference approximation used. However, the error also depends on the number of figures used in the storage of the density. This is an important point because in most of the software currently used, the density is stored only for plotting purposes, with 3−7 significant figures (FN).

To study the effect of the size of h and FN of ρ on the localization and the $-\nabla^2\rho$ value at the critical points of the Laplacian, we have determined the atomic graphs in CO and NO molecules using different values of h and FN on ρ. The results showed that a value of h between 0.04 and 0.02 with a FN value between 7 and 12, guarantees a precision from 4 to 6 FN in the topological analysis of $-\nabla^2\rho$. The distance from the nucleus to the CPs and the $-\nabla^2\rho$ value at the CPs of the VSCC of the C, O, and N atoms of the CO and NO molecules for selected h values and FN equal to 12 are reported in Tables 1 and 2, respectively. Contour maps for $h = 0.02$ are shown in Figure 2. In CO, the carbon atom exhibits only one local charge concentration or (3, −3) type CP, (Vnb), which is located in the nonbonded region. A torus of charge depletion around the internuclear axis with a ring of degenerated points is found in the C VSCC. The O VSCC distribution shows two local charge concentrations located along the C−O bond direction. One is facing the carbon atom (Vb), while the other is found in the opposite side of the shell forming a nonbonded charge concentration (Vnb). The ground state of NO ($^2\pi$) has the open shell configuration $(1\sigma)^2(2\sigma)^2(3\sigma)^2(4\sigma)^2(5\sigma)^2(1\pi)^4(2\pi)$ so that the extra electron in the 2π molecular orbital, that is mostly localized in a plane, destroys the axial symmetry. In NO, both the N and O VSCC show three local maxima, two nonbonded forming an angle of 120° with the bond direction and one located in the bond region. Three (3, −1) critical points lie on the same plane of the (3, −3) forming two faces, one above and the other below the plane, with two (3, +1) capping the atomic graph. Tables 1 and 2 confirm that a value of h around 0.03 and a FN of 12 in ρ produces a good precision (around 10^{-6}) in the localization of and in the topological properties at the critical points of $-\nabla^2\rho$.

To consider a more complex case, we have studied the Cu_{13} cluster. This a model of the (100) Cu surface with the geometrical parameters of the bulk. Cu unit cell is a cubic[41] fcc and belongs to the $Fm3m$ space group with $a = 3.577$ Å. Experimental studies[42] have shown that the (100) Cu surface reconstructs only to a small extent so that the geometry of the first and second layer is essentially unchanged from the bulk one. Previous results[30] have shown that the atomic graph for the central Cu atom (modeling the Cu of the surface) has six vertices, two along the axis perpendicular to the surface, one above (L_u) and other below the surface (L_d), and four (L_i with $i = 1, ..., 4$) in the plane along the Cu−Cu bonds. These CPs are linked by twelve edges, four between the L_u and L_i, four between L_d and L_i, and four linking the L_is. Thus, the atomic graph (Figure 3) of the Cu atoms is an octahedron with eight faces joining the vertices, four above the surfaces and four below it. The distance nucleus CPs and the $-\nabla^2\rho$ value at these critical points for $h = 0.04$ are collected in Table 3. This table shows that, even in this complex case, a value of h around 0.03 offers a good compromise between computational cost and numerical precision (from 10^{-4} to 10^{-6}) in the determination of the atomic graphs and the calculation of the $-\nabla^2\rho$ value at its critical points.

The previous results show that NUMLAP can be applied with confidence to any numerical density regardless of the method employed in the determination of ρ. As an example of its capabilities, we will apply it to carry out the topological analysis of the Laplacian of an electronic density determined using an atomic numerical basis set. In this application, we will study the atomic graph of the Cu and Fe atoms on the (100) Cu and (001) Fe surfaces using the DMOL[43] program ($h = 0.03$ and FN = 10) to generate ρ. The KS numerical orbitals were calculated with the BLYP functional and a double-numerical

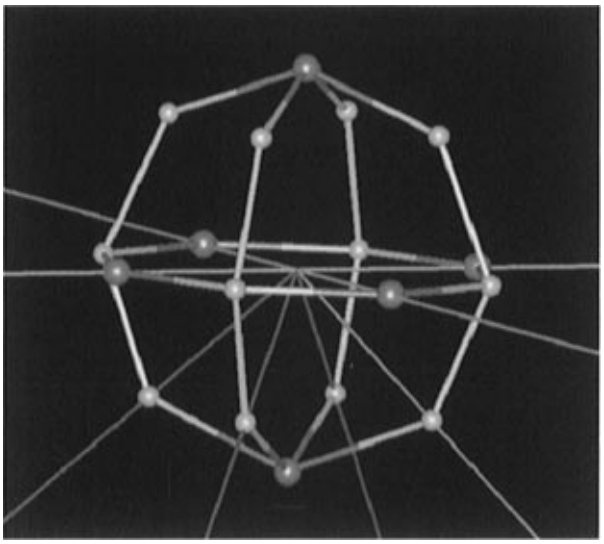

Figure 3. Atomic graph for top atoms in Cu (100) surface. Large gray and small white spheres denote the vertex ((3, −3) CPs) and the edges ((3, −1) CPs), respectively. The graph exposes a vertex perpendicular to the top of the surface.

TABLE 3: Data for Critical Points in the Laplacian of $\rho(\mathbf{r})$ in the Central Top Cu Atom on the Cu_{13} Cluster

critical points	$-\nabla^2\rho$	$\mathbf{r}_{Cu}$
one (3, −3) above surface	60.987 709 77	0.543 557 57
	60.987 694 33	0.543 558 03
one (3, −3) below surface	60.945 407 78	0.543 682 68
	60.945 406 11	0.543 683 11
four (3, −3) in surface	61.252 429 88	0.543 458 69
	61.252 430 43	0.543 458 64
four (3, −1) above surface	57.799 769 06	0.545 378 34
	57.799 770 55	0.543 378 33
four (3, −1) in surface	58.603 741 29	0.544 958 70
	58.603 748 62	0.544 959 14
four (3, −1) below surface	57.203 703 96	0.545 817 76
	57.203 703 65	0.545 817 75
four (3, +1) above surface	56.992 454 61	0.545 849 32
	56.992 455 56	0.545 849 32
four (3, +1) below surface	56.494 608 92	0.546 217 20
	56.494 605 22	0.546 217 17

[a] In each line, the first and second rows give the BUBBLE and NUMLAP results, respectively.

basis set (DNP) including polarization.[6] These are examples of surfaces of fcc and bcc transition metals, respectively.

In bulk[41] Cu, each atom has 12 nearest neighbors at 2.56 Å that are reduced to eight at the top of the (100) surface. We have studied this surface using cluster models containing from two to four layers of Cu atoms parallel to the (100) plane. We have determined, in each case, the critical points of the VSCC of the surface top central atom. The Cu atomic graph is found to exhibit no dependence on the slab depth, and a model containing two layers is sufficient to give the right graph, an octahedron similar to that showed in Figure 3. For that reason, we have reported the results obtained in a Cu_{41} cluster (Figure 4) modeling a periodic slab of two layers. The distance nucleus CPs and the $-\nabla^2\rho$ value at the critical points that generate the regular octahedron previously mentioned and forming the atomic graph are collected in Table 4.

The lattice of bulk[41] Fe is cubic bcc and is described by the *Im*3*m* space group with $a = 2.866$ Å. Each Fe atom has eight first nearest neighbors at 2.48 Å and six second nearest neighbors at 2.87 Å. In the (001) surface top atom, these interactions are reduced to four with its first neighbors (located in the second layer) and five with the second ones (four in the second layer and one in the third layer). Similarly, to the (100) Cu case, experimental[44,45] studies have shown that the (001)

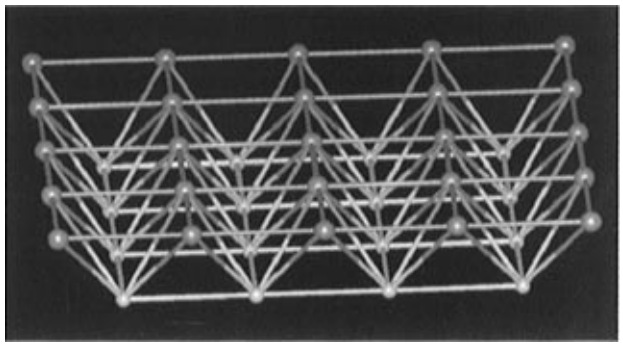

Figure 4. Cu_{41} cluster modeling a slab of two layers of the (100) Cu surface. Gray and white spheres denote a Cu atom on the first and second layer, respectively.

TABLE 4: Data for Critical Points of the Laplacian of $\rho(\mathbf{r})$ in the Central Top Cu Atom of the Cu_{41}

critical points	$-\nabla^2\rho$	$\mathbf{r}_{Cu}$
one (3, −3) above surface	63.5515	0.5325
one (3, −3) below surface	65.2372	0.5315
four (3, −3) in surface	64.0215	0.5321
four (3, −1) above surface	58.9510	0.5345
four (3, −1) in surface	61.9747	0.5330
four (3, −1) below surface	59.4690	0.5341
four (3, +1) above surface	58.4289	0.5347
four (3, +1) below surface	58.821	0.5344

TABLE 5: Data for Critical Points of the Laplacian of $\rho(\mathbf{r})$ in the Central Top Fe Atom of the Fe_{21} Cluster

critial points	$-\nabla^2\rho$	$\mathbf{r}_{Fe}$
four (3, −3) above surface	30.2286	0.6017
four (3, −3) below surface	30.0282	0.6285
four (3, −1) above surface	28.9801	0.5988
four (3, −1) in surface	29.3331	0.6167
four (3, −1) below surface	28.5089	0.6345
one (3, +1) above surface	26.4221	0.5950
four (3, +1) in surface	25.2640	0.6210
one (3, +1) below surface	25.1176	0.6555

Fe surface does not reconstruct, with a probable contraction of 1.4% in the first layer. Thus, we have studied this surface using cluster models containing from two to four layers of Fe atoms parallel to the (001) plane with the same geometrical parameters of the bulk. As in the Cu case, the Fe atomic graph exhibits no dependence on the slab depth so a two layer model gives the right graph. The data for the critical points of $-\nabla^2\rho$ in the VSCC of the top central Fe atom for a Fe_{25} cluster model (Figure 5a) are reported in Table 5. The atomic graph so defined is a cube (Figure 5b) with eight vertices, four above and four below the surface, linked by 12 edges and six faces joining those vertices. Thus, the atomic graph of the Fe atom shows, with respect the Cu one, dramatic changes. The magnitude of the $-\nabla^2\rho$ at the CPs changes from around 60 au in Cu, a nearly filled d-band case, to around 30 au in Fe, a nearly half-filled d-band case. The atomic graph of the Cu atom exhibits a (3, −3) CP type, a local maximum above the surface while Fe atom exposes a (3, +1) CP, a local minimum in the VSCC. Therefore, the VSCC of the Cu and Fe atoms expose, above the surface, a "peak" and a "hole" of charge, respectively. These drastic variations in the Laplacian distribution are closely related to the opposite reactivity behavior shown by the Cu and Fe surfaces toward a molecule such as CO. It is known that the CO molecule does not remain[46] on the Cu surface at room temperature while it is dissociatively absorbed[47] on Fe surface. The perpendicular bonding of the CO molecule through the C atom on the surface of Cu would require that a vertex on CO interacts with a vertex (a repulsive interaction) on the surface. The bonding on Fe corresponds to a vertex (adsorbate)−face (surface) interaction, an attractive interaction.

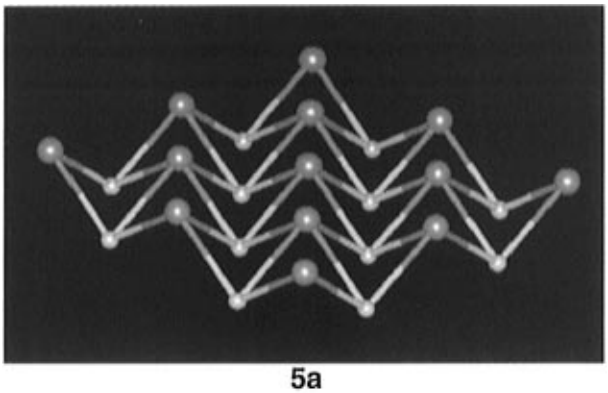

5a

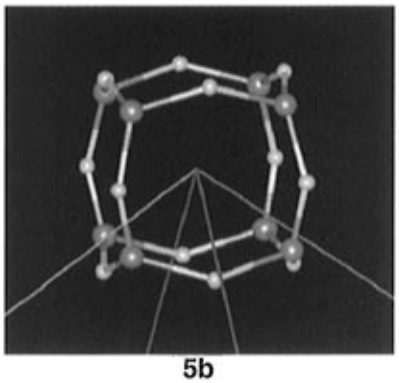

5b

Figure 5. (a) Fe_{21} cluster modeling a slab of two layers of the (001) Fe surface. Gray and white spheres denote Fe atom on the first and second layer, respectively. (b) Atomic graph for top atoms in Fe (001) surface. Large gray and small white spheres denote the vertex and the edges, respectively. The graph exposes a face perpendicular to the top of the surface. The lines indicate the bond direction with the atoms of the second layer of the surface.

Conclusions

A numerical method to perform the topological analysis of the Laplacian of $\rho(\mathbf{r})$ regardless of how it was generated (analytically, numerically, or even experimentally) was implemented for the BUBBLE program. The method allows, for example, the study by DFT by complex systems where the electronic correlation is important, regardless the kind of basis set used, and allows to predicts the chemical reactivity with the atomic graphs of the topological theory of Bader. It would be equally simple to adapt this method to other available programs, such as the MORPHY program.

Acknowledgment. The authors thank Dr. Juan Rivero Charlton and Dr. Juan Murgich for their valuable help in linguistic matters.

References and Notes

(1) Lundqvist, S., March, N. H., Eds. *Theory of the Inhomogeneous Electron Gas*; Plenum Press: New York, 1983.
(2) Parr, R. G.; Yang, W. *Density-Functional Theory of Atoms and Molecules*; Oxford University Press: New York, 1989.
(3) Perdew, J. P.; Chevary, J. A.; Vosko, S. H.; Jackson, K. A.; Pederson, M. R.; Singh, D. J.; Fiolhais, C. *Phys. Rev.* **1992**, *B46*, 6671.
(4) (a) Andzelm, J.; Wimmer, E. *J. Chem. Phys.* **1992**, *96*, 1280. (b) Andzelm, J.; Baker, J.; Scheiner, A.; Wrinn, M. *Int. J. Quantum Chem.* **1995**, *56*, 734.
(5) Jones, R. O.; Gunnarson, O. *Rev. Mod. Phys.* **1989**, *61*, 689.
(6) Belley, B. *J. Chem. Phys.* **1990**, *92*, 508.
(7) Harris, F. E.; Koures, A. G. *Int. J. Quantum Chem., Quantum Chem. Symp.* **1995**, *29*, 235.
(8) Seminario, J. M., Politzer, P., Eds. *Modern Density Functional Theory: A Tool for Chemistry*; Elsevier: New York, 1995.
(9) Ruette, F., Ed. *Quantum Chemistry Approaches to Chemisorption and Heterogeneous Catalysis*; Kluwer Academic Publishers: Boston, 1992.
(10) Bader, R. F. W. *Atoms in molecules − a quantum theory*; Claredon Press: Oxford, U.K, 1990.
(11) Bader, R. F. W. *Phys. Rev.* **1994**, *B49*, 13 348.
(12) Bader, R. F. W. *Acc. Chem. Res.* **1985**, *18*, 9.
(13) Wiberg, K. B.; Bader, R. F. W.; Lau, C. D. H. *J. Am. Chem. Soc.* **1987**, *109*, 985.
(14) Popelier, P. L. A.; Bader, R. F. W. *Chem. Phys. Lett.* **1992**, *189*, 542.
(15) Zou, P. F.; Bader, R. F. W. *Acta Crystallogr.* **1994**, *A50*, 714.
(16) Tsirelson, V. G.; Zou, P. F.; Tang, T.-H.; Bader, R. F. W. *Acta Crystallogr.* **1995**, *A51*, 143.
(17) Boyd, R. J.; Choi, S. C. *Chem. Phys. Lett.* **1985**, *120*, 80.
(18) Eberhart, M. E.; Donovan, M. M.; McLaren, J. M.; Clougherty, D. P. *Prog. Surf. Sci.* **1991**, *3*, 1.
(19) Eberhart, M. E.; Clougherty, D. P.; McLaren, J. M. *J. Mater. Res.* **1993**, *8*, 438.
(20) Bader, R. F. W.; Essén, H. *J. Chem. Phys.* **1984**, *80*, 1943.
(21) Bader, R. F. W.; MacDougall, P. J.; Lau, C. D. H. *J. Am. Chem. Soc.* **1984**, *106*, 1594.
(22) Bader, R. F.; MacDougall, P. J. *J. Am. Chem. Soc.* **1985**, *107*, 6788.
(23) Bader, R. F. W.; Popelier, P. L. A.; Chang, C. *J. Mol. Struct.:* THEOCHEM **1992**, *255*, 145.
(24) Sagar, R. P.; Ku, A. C. T.; Smith, V. H., Jr. *J. Chem. Phys.* **1988**, *88*, 4367.
(25) Shi, Z.; Boyd, R. J. *J. Chem. Phys.* **1988**, *88*, 4375.
(26) Carrol, M. T.; Chang, C.; Bader, R. F. W. *Mol. Phys.* **1988**, *63*, 387.
(27) Aray, Y.; Bader, R. F. W. *Surf. Sci.* **1996**, *351*, 233.
(28) Aray, Y.; Rosillo, F.; Murgich, J. *J. Am. Chem. Soc.* **1994**, *116*, 10 639.
(29) Aray, Y.; Rodriguez, J.; Murgich, J.; Ruette, F. *J. Phys. Chem.* **1993**, *97*, 8393.
(30) Aray, Y.; Rodriguez, J. *Can. J. Chem.* **1996**, *74*, 1014.
(31) Krugg, P.; Bader, R. F. W. Department of Chemistry, McMaster University: Hamilton, Ontario, 1990.
(32) *Gaussian 94*, Revision B.3, M. J. Frisch, G. W. Trucks, H. B. Schlegel, P. M. W. Gill, B. G. Johson, M. A. Robb, J. R. Cheeseman, T. Keith, G. A Peterson, J. A. Montgomery, K. Raghavachari, M. A. Al-Laham, V. G. Zakrzewski, J. B. Ortiz, J. B. Foresman, C. Y. Peng, P. Y. Ayala, W. Chen, M. W. Wong, J. L. Andres, E. S. Replogle, R. Gomperts, R. L. Martin, B. J. Fox, J. S. Binkley, D. J. Defrees, J. Baker, J. O. Steward, M. Head-Gordon, C. Gonzalez, and J. A. Pople.
(33) Cioslowski, J.; Nanayakkara, A. *Chem. Phys. Lett.* **1994**, *219*, 151.
(34) Popelier, P. L. A. *Chem. Phys. Lett.* **1994**, *228*, 160.
(35) Gatti, C.; Saunders, V. R.; Roetti, C. *J. Chem. Phys.* **1994**, *101*, 10 686.
(36) Dovesi, R.; Saunders, V. R.; Roetti, C. Theoretical Chemistry Group, University of Turin: Italy and Daresbury Laboratory, U.K. 1992.
(37) Al-Khafaji, A. W.; Tooley, J. R. *Numerical Methods in Engineering Practice*; Holt, Rinehart and Winston Inc.: New York, 1986; *Handbook of Mathematical Functions with Formulas, Graphs and Mathematical Tables*; Abramowitz, M., Stegun, A., Eds.; National Bureau of Standars Applied Mathematical Series 55, 1964.
(38) Becke, A. D. *J. Chem. Phys.* **1988**, *88*, 2547.
(39) Lee, C.; Yang, W.; Parr, R. G. *Phys. Rev.* **1988**, *B37*, 786.
(40) Krishnan, R.; MFrisch, M. J.; People, J. A. *J. Chem. Phys.* **1980**, *72*, 4244.
(41) Moruzzi, V. L.; Janak, J. F.; Williams, A. R. *Calculated Electronic Properties of Metals*; Pergamon Press: New York, 1978.
(42) (a) Lind, D. M.; Dunning, F. B.; Walters, G. K.; Davis, H. L. *Phys. Rev.* **1987**, *B35*, 9037. (b) Lindgren, S. A.; Wollden, L.; Rundgren, J.; Westrin, P. *Phys. Rev.* **1984**, *B29*, 576.
(43) *Dmol/Dsolid*, Release 3.0 and 95.0; Biosym/MSI Inc.: San Diego, 1995.
(44) Marchut, C.; Buck, T. M.; Wheatley, G. A.; McMahon, C. *Surf. Sci.* **1984**, *141*, 549.
(45) Legg, K. O.; Jona, F.; Jopsen, D. W.; Marcus, P. M. *J. Phys. C: Solid State Phys.* **1977**, *10*, 937.
(46) Yu, K. Y.; Spicer, W. E.; Lindau, I.; Pianetta, P.; Lin, S. F. *Surf. Sci.* **1976**, *57*, 157.
(47) Jona, F.; Legg, K. O.; Shih, H. D.; Jepsen, D. W.; Marcus, P. M. *Phys. Rev. Lett.* **1978**, *40*, 1466.